Polymer Testing 93 (2021) 106986

Contents lists available at ScienceDirect

Polymer Testing

journal homepage: http://www.elsevier.com/locate/polytest

Synthesis of sustainable, lightweight and electrically conductive polymer brushes grafted multi-layer graphene oxide

Héctor Aguilar-Bolados [a,*], Mehrdad Yazdani-Pedram [b], Eduardo Quinteros-Jara [b], Quimberly Cuenca-Bracamonte [b], Raúl Quijada [a], Javier Carretero-González [c], Francis Avilés [d], Miguel A. Lopez-Manchado [c], Raquel Verdejo [c]

[a] Facultad de Ciencias Físicas y Matemáticas, Universidad de Chile, Beauchef 850, 8380492, Santiago, Chile
[b] Facultad de Ciencias Químicas y Farmacéuticas, Universidad de Chile, Olivos 1007, 8380544, Santiago, Chile
[c] Instituto de Ciencia y Tecnología de Polímeros, ICTP-CSIC, Juan de la Cierva, 3 28006, Madrid, Spain
[d] Centro de Investigación Científica de Yucatán, A.C., Unidad de Materiales, Calle 43 # 130, Chuburná de Hidalgo, 97205, Mérida, Yucatán, Mexico

ARTICLE INFO

Keywords:
Polymer brushes
Multi-layer graphene oxide
Surface-initiated controlled radical polymerization
ARGET-ATRP
Sustainable resources

ABSTRACT

This work reports the synthesis of poly (monomethyl itaconate) grafted multi-layer graphene oxide (PMMI-g-GO) by atom transfer radical polymerization using activators regenerated by electron transfer (ARGET-ATRP). PMMI-g-GO presents outstanding properties, such as a high electrical conductivity (5.04 S m^{-1}), low number of stacked graphene layers (6) and I_G/I_{2D} ratio of 2.05 estimated from Raman spectrum, which indicates the high quality of PMMI-g-GO as a graphenic material. In addition, polymer brushes based on PMMI represent a new green alternative for the development of polymer composite materials, since the monomer used for their production is obtained from a renewable source. Interestingly, the PMMI-g-GO nanomaterial is also capable of storing Li^+ ions without the need of using electron conductive additives that are usually employed in the electrode's composition of conventional lithium ion batteries.

1. Introduction

The end of the last century and the beginning of this one were strongly marked by the advent of carbonaceous nanomaterials. Fullerenes [1], carbon nanotubes [2], graphene [3], among others [4] have aroused as materials which could lead the development of scientific and technological advances in several fields. A building block for all these carbon materials is graphene [3]. Graphene is a single carbon atom layer where the atoms are linked by sp^2 bonds in a long-range hexagonal lattice. A consequence of this arrangement is the in-plane π-conjugation, which imparts outstanding properties. This fact makes graphene a highly promising material for a wide range of applications, which can be found in the following reviews [5–8]. This is one of the main reasons why researchers worldwide have shown an enormous interest for developing efficient methods for producing graphene in the gram-scale. The high scientific activity on graphene has sped up the creation of new members of the graphene's family [9]. Few-layered graphene, graphene quantum dots, graphene nanoribbons, graphene oxides, functionalized graphene and doped graphene are part of this graphene's family [10]. Among the extraordinary properties exhibited by graphene, it is important to highlight its electrical conductivity, which can be as high as that exhibited by metals, and its thermal conductivity, higher than that of diamond or single-wall carbon nanotubes [11–14]. Therefore, graphenic materials have been used for a number of applications, such as smart polymers, membranes, pyroelectric sensors, among others [15–20]. From these potential applications several examples already exist in the market such as conducting additives in electrode materials for batteries, additives in anti-corrosion primes, precursor for thermal dissipation films or touch panels and thermal heaters [21]. Among the family of graphenic materials, graphene oxides have become an important substrate for obtaining interesting functionalized graphenic materials. This is due to the fact that graphene oxide can be subjected to different chemical reactions, such as reductive amination and fluorination [22,23].

Several researchers have addressed the use of graphenic material as filler for preparing polymer nanocomposites [24–27], since the resulting nanocomposites could show high electrical conductivity with improved mechanical properties by using small concentrations of filler [25,28].

* Corresponding author.
E-mail address: haguilar@ciq.uchile.cl (H. Aguilar-Bolados).

https://doi.org/10.1016/j.polymertesting.2020.106986
Received 12 July 2020; Received in revised form 28 October 2020; Accepted 23 November 2020
Available online 27 November 2020

One of the critical aspects to obtain these improvements is to achieve an optimum dispersion of the filler in the polymer matrix. Therefore, graphenic material is frequently covalently or non-covalently functionalized in order to increase its compatibility with the polymer. The former targets the formation of covalent bonds between the graphenic material and other molecular entities, whereas the latter only seeks the surface modification of graphene by the formation of intermolecular interactions between graphene and other molecules [29]. The non-covalent modification is usually carried out using surfactants [24]. One of the advantages of covalent functionalization is that prevents the migration of molecules from the graphene surface. The surface-initiated controlled radical polymerization (SI-CRP) is a versatile approach for modifying the material surface by a grafting reaction, generating individual polymer chains linked by one of their ends to the surface. This type of structure is known as polymer brush [30]. Surface-initiated atom transfer radical polymerization (SI-ATRP) is the most widely used SI-CRP method, because through easy steps using routine laboratory equipment it is possible to modify drastically the surface character of a wide range of different materials. SI-ATRP is a "grafting from" process since, previous to polymerization, the surface of the material is functionalized with the dormant species that will initiate the polymerization under specific reaction conditions. One of the most used initiators is 2-bromoisobutyryl bromide (BIBB), given that the acyl bromide and bromine groups are susceptible to nucleophilic attack at tertiary carbon, where the polymerization reaction is initiated [31]. Recently, a subclass of ATRP has been reported, which considers the use of activators regenerated by electron transfer (ARGET-ATRP) of vinyl compounds. ARGET-ATRP is especially versatile and requires lower amount of catalyst compared to conventional ATRP [32].

Several authors have reported strategies of modifying graphene oxide in order to obtain an ATRP macro-initiator [31,33–35]. An interesting and easy strategy consists in silanization using compounds having double functionality at the ends, namely alkoxy-silane and primary amine groups. Alkoxy-silane groups are susceptible to react with the hydroxyl groups present in graphene oxide [36]. As a result of the silanization of graphene oxide, primary amine groups are available on its surface. The primary amines of silanized graphene oxide can undergo nucleophilic substitution reaction with acyl bromide groups of BIBB, as shown in Fig. 1.

The use of functionalized graphene oxide as a macro-initiator in ATRP reactions has already been reported in the literature [37,38]. Styrene and acrylates are the most commonly used as monomers in ATRP reactions; although in recent years, other more economical and environmentally friendly alternatives are being evaluated [39–41]. In this regard, methylene succinic acid and its derivatives are seen as a sustainable alternative, since it is obtained from sugars by fermentation from *aspergillus terreus* and *aspergillus itaconicus* [42]. Methylene succinic acid, also known as itaconic acid, is a dicarboxylic acid with a vinyl function. In spite of the susceptibility of vinyl function to react by radical polymerization, this is inhibited by the presence of carboxylic acid, which is an electron-withdrawing group [43]. However, 4-methyl methylene succinate (also known as monomethyl itaconate, a derivative of itaconic acid) is a monomer that is more susceptible to polymerize by free radical reactions because ester groups have a lower electron-withdrawing character than carboxylic acid groups. In addition, it is known that the ATRP technique allows to polymerize monomers, that have electron-withdrawing groups in their structure, more easily than classical free radical polymerization [44]. This work reports on the synthesis of multi-layer graphene oxide functionalized with poly (monomethyl itaconate) using the ARGET-ATRP technique (Fig. 2). This material has interesting structural and morphological characteristics and a high electrical conductivity. Hence, considering these characteristics, the potential applications of this material are plentiful. First, the functionalization of graphene oxide with a monomer obtained from a non-fossil feedstock can contribute to the development of a new sustainable functionality. Likewise, the presence of carboxylic acid and ester as side groups should also enable further modifications or covalent bonds to other polymers. Secondly, and most importantly, the high electrical conductivity of the functionalized graphene material could be used for the development of lightweight and flexible electronic materials, which have a myriad of applications from sensors, to wearables, solar cells, supercapacitors, or electrodes. Here, we explore its use as electrodes for Li ion batteries [45].

2. Experimental

2.1. Materials

Natural graphite (NG) flakes (100 mesh), fuming nitric acid (≥99.0%), potassium chlorate (≥99.0%), (3-aminopropyl)triethoxysilane (APTES) (≥98.0%), α-Bromoisobutyryl bromide (BIBB) (98.0%), triethylamine (≥98.0%), Copper(II) bromide ($CuBr_2$), N,N,N′,N′′,N′′-Pentamethyldiethylenetriamine (PMDETA, 99%), ascorbic acid (≥99.0%), dimethylformamide (DMF) and toluene were supplied by Sigma-Aldrich (USA). Methylene succinic acid methyl ester (monomethyl itaconate) was synthesized from methylene succinic acid (≥99.0%) and a sample of poly(monomethyl itaconate) (PMMI), as a control sample, was prepared by using dibenzoyl peroxide using a previously reported methodology [46].

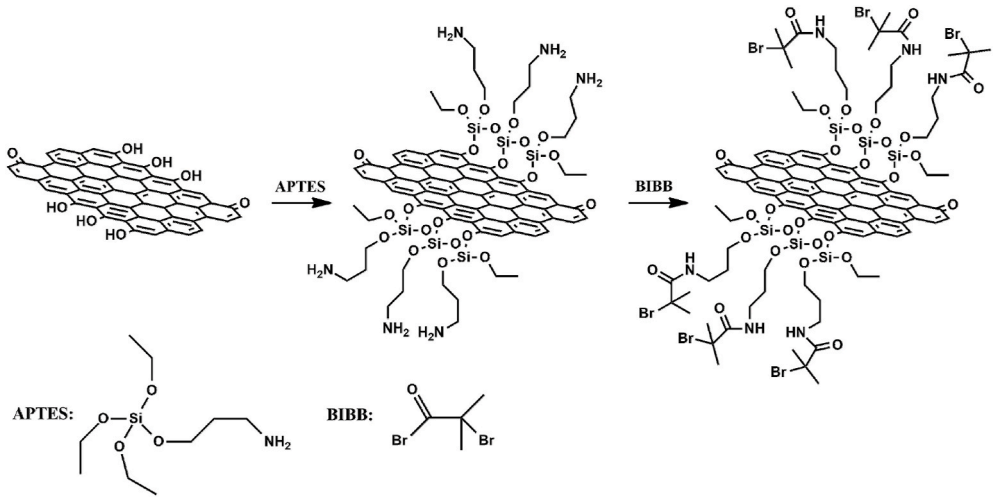

Fig. 1. Scheme of graphene oxide functionalization reaction to obtain the ARGET-ATRP macro-initiator.

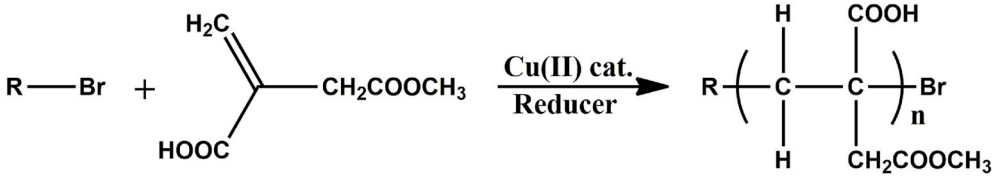

Fig. 2. Scheme of ARGET-ATRP reaction using monomethyl itaconate.

2.2. Synthesis of graphene oxide

Graphene oxide (GO) was obtained using Brodie's method, which involved the addition of 12 g of graphite, and 240 ml of fuming nitric acid to a temperature-controlled reactor at 0 °C. Subsequently, 96 g of potassium chlorate were slowly added to the reactor. This mixture was left under stirring for 22 h. After reacting, the crude product was washed with abundant distilled water and the graphene oxide was recovered by washing and centrifugation cycles until the supernatant reached pH = 6. The purified graphene oxide with sludge appearance was dried at 70 °C for 12 h.

2.3. Silanization of graphene oxide

Silanized graphene oxide (GO-S) was obtained in two steps. First, a suspension of 5 g of GO in 50 ml of toluene was sonicated using a Q700 ultrasonic equipment (Qsonica, USA) for 30 min, 300 W and below 30 °C. Subsequently, this suspension was added to a reactor, which was sealed and purged using nitrogen gas and the temperature was set at 0 °C. Then, 1 ml of (3-aminopropyl)triethoxysilane was added to the reactor. After 3 h of reaction at 0 °C, the temperature was raised to 90 °C and the reaction was continued for 3 h. Once the reaction was concluded, the solid product was washed using toluene and filtered under vacuum. Then, the material was dried in a vacuum oven at 70 °C for 18 h.

2.4. Synthesis of multi-layer graphene oxide ATRP macro-initiator

Graphene oxide ATRP macro-initiator (GO-SB) was synthetized by the dispersion of 5 g of GO-S in 50 ml of dried DMF and sonicated at 70 W for 30 min. Then, this mixture was added to a temperature-controlled reactor, which was sealed and purged with nitrogen gas. Subsequently, 1.5 ml of α-Bromoisobutyryl bromide and 0.9 ml of triethylamine were added to the reaction mixture and was left to react for 3 h at 0 °C. Then, the temperature of the reaction was raised to 100 °C, keeping the reaction for 21 h. Once the reaction was concluded, the resulting suspension was vacuum filtered and the solid was washed with DMF and dried at 40 °C for 24 h.

2.5. Synthesis of poly(monomethyl itaconate) grafted multi-layer graphene oxide

Poly(monomethyl itaconate) grafted graphene oxide (PMMI-g-GO) was synthesized by ARGET-ATRP using GO-SB as macro-initiator and monomethyl itaconate as monomer. 200 ml of toluene, 3.6 GO-SB, 20 g of MMI, 7.8 mg of $CuBr_2$ and 0.581 g of ascorbic acid were added to a three neck 500 ml round bottom flask and purged using nitrogen gas. The reaction temperature was set to 80 °C. Then, PMDETA was added and left to react for 24 h. Then, the solvent was removed using a rotary evaporator. The reaction product was dialyzed using a membrane tubing of 2 KDa (MWCO) and deionized water at room temperature for 72 h in order to eliminate the unreacted monomer, catalyst and low molecular weight by-products. Then, the purified solid product was removed from the dialysis membrane tubing and dried at 70 °C for 12 h. The mass of the product was 7.02 g.

2.6. Characterization

X-ray diffraction analysis of the different graphenic materials was carried out using a Bruker diffractometer model D8 Advance (Massachusetts, USA) with a Cu Kα radiation source, wavelength λ = 0.154 nm and power supply of 40 kV and 40 mA. The incident angle (2θ) was varied between 4° and 80° and the scan rate was 0.02°/s. The interlayer distance, crystallite size and number of stacked layers were estimated using a previously reported procedure [23].

The graphenic material was also characterized by Raman spectroscopy using a Renishaw InVia Raman microscope equipped with a 514.5 nm wavelength laser and 0.02 cm^{-1} resolution. The spectra were recorded from 400 to 4000 cm^{-1}. The inter-defect distance of the different graphenic materials was estimated using a methodology reported previously [23].

Thermogravimetric analysis (TGA) was carried out in the temperature range from 25 °C to 800 °C at a heating rate of 10 °C/min in nitrogen atmosphere using a Netzsch thermogravimetric analyzer model Iris TG 209 F1.

The morphology of the samples was analysed by scanning electron microscopy, JEOL-Oxford Instruments IT3000, and high resolution scanning electron microscopy, Hitachi S8000 with field emission filament.

X-ray photoelectron spectroscopy (XPS) of PMMI-g-GO was carried out using a PerkinElmer XPS–Auger spectrometer, model PHI 1257 (Massachusetts, USA), which includes an ultra-high vacuum chamber, a hemispheric electron energy analyzer and X-ray source with Kα radiation unfiltered from an Al (hν = 1486.6 eV) anode. The measurements were performed at 400 W and emission angle of 70° to obtain information from the deep surface. The determination of carbon and oxygen functional groups was carried out by fitting the C1s and O1s peaks. The baseline model corresponded to a *Shirley* model and curve fitting was conducted with Lorentz curves.

The electrical conductivity and dielectric permittivity at room temperature were determined using a high-resolution Alpha-Novocontrol dielectric spectrometer. A disk of PMMI-g-GO was placed in the dielectric cell between two parallel gold electrodes. The disk was prepared by pressing into a special cast.

The lithium ion storage capacity of PMMI-g-GO, when used as electrode material, was carried out by using stainless steel symmetric Swagelok® half-cell. For this, the PMMI-g-GO material in the form of fine powder was dried under vacuum at 70 °C overnight. Then, it was transferred to an Argon glove box (H_2O < 5 ppm, O_2 < 5 ppm) and assembled as positive electrode in a symmetric two-electrode configuration with a disc of metallic lithium as negative electrode and a porous glass fiber disc (Whatman®) acting as a separator to avoid electric shortcut. The separator was previously impregnated with a commercial electrolyte solution with a concentration of 1 M of $LiPF_6$ salt in ethyl carbonate (EC) and dimethyl carbonate (DMC) mixture with a 1:1 vol ratio (Sigma-Aldrich). The Li//electrolyte//PMMI-g-GO cells were galvanostatically cycled in a VMP-300 multichannel potentiostat/galvanostat (Bio-Logic) in a voltage range between 0.005 V and 3.0 V vs Li^+/Li operating at constant current densities.

3. Results and DISCUSSION

3.1. Structure of PMMI-g-GO

Fig. 3 shows the normalized X-ray diffraction patterns of NG, GO, GO-S, GO-SB and PMMI-g-GO. It is observed that NG presents an intense peak at 26.2° (d = 3.40 Å), which corresponds to the (002) reflection plane, characteristic of graphitic materials. The number of stacked layers (N_L) estimated for NG is around 54. As a result of the oxidation process, the diffraction peak associated to the (002) plane no longer appears in the GO diffraction pattern. Instead, GO presents an intense diffraction peak at 15.1° (d = 5.87 Å) and a decrease of the number of stacked layers (N_L = 22), as shown in Table 1. This indicates that the oxidation process of graphite was successful, since the presence of oxygenated functional groups increases the interlayer distance. An interesting fact is observed as consequence of the silanization process, since two new diffraction peaks are observed at 6.19° (d = 14.3 Å) and 12.5° (d = 7.10 Å). This increase of interlayer distance suggests that the graphene oxide layers were successfully functionalized by the silane agent (APTES).

As a result of the reaction between the primary amine bounded to a sp^3 terminal carbon of GO-S and the acyl bromide groups present in BIBB, GO-SB show diffraction peaks slightly shifted to lower angles, 6.11° (d = 14.5 Å) and 11.9° (d = 7.4 Å), respectively. The appearing of a broad peak *ca.* 25.4°, being more intense than those observed at 6.11° and 11.9°provides evidence of the partial recovery of the graphitic structure. This suggests that the nucleophilic substitution reaction has occurred. In addition, the recovering of π-conjugated system suggests the reduction of graphene oxide. ARGET-ATRP reaction between GO-SB and monomethyl itaconate results in a PMMI-g-GO, which presents peaks shifted to lower angles than those observed in GO-SB, suggesting the occurrence of the controlled polymerization reaction. The discrete increase of the interlayer distance of PMMI-g-GO could be associated to the fact that the polymerization reaction occurs by the bromine groups located in the terminal sp^3 carbon atoms.

Fig. 4 shows the Raman spectra of the investigated materials, where characteristic absorption bands of graphenic materials are observed. The *D* and *D′* bands, associated with the breathing modes due to inter-valley process of double resonance, appear *ca.* 1350 cm^{-1} and *ca.* 1620 cm^{-1}, respectively [47]. The *G* band corresponding to the first-order scattering of the E_{2g} phonon mode of sp^2 carbon atoms appears around 1580 cm^{-1}. The 2D band, *ca.* 2700 cm^{-1}, corresponds to an overtone of *D* band; while the combination of the overtones of *D* and *D′* bands, called *D* + *D′* band, appears around 2920 cm^{-1} [47]. NG presents an intense and narrow *G* band at 1566 cm^{-1} and a small *D* band, suggesting that NG has low defects density (I_D/I_G) with an inter-defect distance (L_D) of 226 nm (Table 1). Conversely, GO presents a wide and intense *D* band, which indicates the presence of oxygenated functional groups and defects [48]. This is reflected in the increase of the I_D/I_G ratio to 0.76 and the significant decrease of the inter-defect distance (L_D = 22 nm) as a consequence of the oxidation, which promotes the degradation of graphene lattice and the incorporation of oxygen functional groups [22,23]. The silanization of GO (GO-S) further increases the I_D/I_G to 1.01 and decreases the L_D to 16 nm. However, an interesting fact is that the *G* band has a Raman blue shift from 1587 cm^{-1} for GO to 1578 cm^{-1} for GO-S. Raman red or blue shifts of the *G* band of functionalized graphene are associated with the electronic effect of the functional groups [49]. Electron-donor groups produce shifts to lower frequencies (Raman red shift), while the electron-acceptor groups produce shifts to higher frequencies (Raman blue shift) [50,51]. Das et al. reported that the interaction of reduced graphene oxide with electron-donor and -acceptor molecules such as aniline and nitrobenzene produces a red-shift or blue shift of G band, respectively [52]. Blue shift of *G* band up to 1627 cm^{-1} was also reported by Zhao et al., who studied the preparation and properties of graphite intercalated compounds (GIC) using $FeCl_3$, which has electron-acceptor character [53]. The Raman blue shift in GO-S could be associated to the fact that oxygen-bounded to silicon atoms by pπ - dπ interactions sharply increase the electronegativity of silyl group, favouring its electron-accepting capacity [54]. GO-SB exhibits a clear change in the shape and intensity of the peaks, reflecting the structural changes that occurred during this step. The width of *D* and *G* bands decreases, the intensity of the *2D* band is significantly increased, and it is possible to observe *D′* band. These changes suggest that the reaction between BIBB and GO-S not only leads to a nucleophilic substitution between acyl bromide groups of BIBB and the primary amine groups presents in GO-S, but also suggests the reduction of the oxygenated functional groups. The increase of *2D* band indicates the recovery of conjugated π system [55], which is attributed to the occurrence of the oxygen reduction. Likewise, the presence of *D′* band and 2 s order bands, *2D* band and *D* + *D′* band, imply the partial recovery of the π-conjugation of the basal plane, since their presence indicates the occurrence of double resonant processes [47], which involve one phonon (*D* and *D′*) and two phonons (2*D* and *D* + *D'*). It is important to note that GO-SB shows an estimated value of I_G/I_{2D} of 2.04, associated with few-layers graphenic materials [56]. Nevertheless, the estimated value of I_D/I_G of 1.05 suggests the presence of functional groups because of the subsequent reaction of functionalization. PMMI-g-GO presents similar characteristics as GO-SB, which could be due to the ARGET-ATRP reaction that took place in dormant species corresponding to the bromide function of terminal carbon of BIBB agent [57].

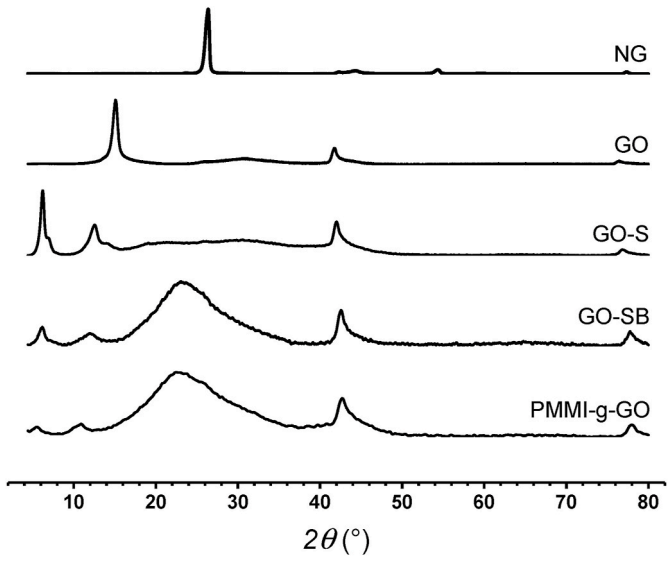

Fig. 3. X-ray diffraction analysis of the different graphenic materials.

X-ray photoelectron spectroscopy survey of PMMI-g-GO is shown in Fig. 5a. The contributions of spectral lines associated to C1s, N1s, O1s and Si2p are observed. The presence of Si2p and N1s suggest that the silanization reaction took place. The lack of spectral lines associated to copper and bromide, indicates that the dialysis method was effective and the catalyst and bromine were completely removed. The main components of PMMI-g-GO are carbon and oxygen, therefore C1s and O1s spectral lines were deconvoluted using Gaussian curves. The C1s peak was satisfactorily fitted to three components (Fig. 5b). The most intense peaks at 286.3 eV and 288.1 eV are assigned to –(CO)–*O*–C*H_3, and -(C*O)–*O*–CH_3 species, respectively, while a lower component around 291.7 eV is associated to –(C*O)–OH functional groups [58–60]. This suggests that the surface of graphene oxide is covered by a layer of PMMI which impedes the detection of π-π*, sp^2 and sp^3 contributions, typically related to graphenic materials [61]. O1s spectral line is presented in Fig. 5c, where three contributions at 534.2 eV, 535.2 eV and 536.1 eV are observed. These contributions are attributed to ester and carboxylic acid groups [60,62]. Contributions at lower binding energy, typically associated to contributions of carbonyl (*ca.* 530.7 eV), hydroxyl (*ca.*

Table 1
Structural characteristics of different graphenic materials determined by X-ray diffraction analysis and Raman spectroscopy.

	X-ray Diffraction Analysis							Raman Spectroscopy						
	(00*l*)				(*h*00)									
	2θ (°)	*d* (A)	D_{00l} (A)	N_L	2θ (°)	*d* (A)	D_{h00} (A)	*D* band (cm^{-1})	*G* band (cm^{-1})	*D′* band (cm^{-1})	*2D* band (cm^{-1})	I_D/I_G	I_G/I_{2D}	L_D
NG	26.2	3.40	180	54	42.3	2.13	233	1344	1566	1604	2696	0.07	3.37	228
GO	15.1	5.87	122	22	41.8	2.16	276	1353	1578	–	2684	0.76	5.52	22
GO-S	6.19	14.3	118	19	42.0	2.15	243	1344	1587	–	2684	1.12	4.34	15
	12.5	7.10	92.3	14										
GO-SB	6.11	14.5	118	9	42.6	2.12	191	1345	1575	1610	2686	1.05	2.04	16
	11.9	7.43	38.9	6										
	25.4	3.50	6.70	3										
PMMI-g-GO	5.45	16.2	41.5	6	42.8	2.11	157	1344	1572	1606	2685	1.05	2.05	16
	10.6	8.32	42.5	6										
	25.5	3.49	5.30	3										

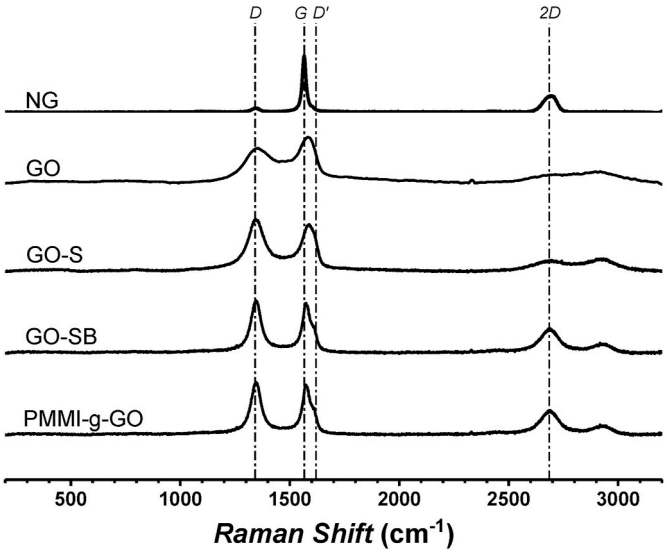

Fig. 4. Raman spectroscopy of the different graphenic materials.

532.3 eV), or ether (*ca.* 533.7 eV) groups are not observed [23]. This fact indicates the presence of a layer of PMMI covalently bonded to graphene oxide that masks the contribution of other oxygenated functional groups.

3.2. Morphology of PMMI-g-GO

Fig. 6a and b shows the SEM images of GO and PMMI-g-GO, respectively, where drastic differences are observed. GO presents a morphology of flakes densely stacked, typical for this material [63], while the grafting reaction leads to flakes randomly oriented with low stacking. This suggests that surface-initiated controlled polymerization promotes the de-stacking of graphene layers. In addition, grafted PMMI brushes onto GO surface decreases the size of flakes, associated to a decrease of the grain size and crystallinity loss as previously observed by X-ray diffraction analysis. STEM image (Fig. 6c) reveals that the low electron density material surrounding the graphene layers corresponds to the grafted polymers brushes. Lee et al. [64] reported a similar morphology when grafting polymer brushes based on polystyrene, poly (methyl methacrylate) or poly(butyl acrylate) onto graphene oxide surface by using a controlled radical polymerization.

3.3. Thermogravimetric analysis

Fig. 7 shows the thermogravimetric analysis of different graphenic materials and a control sample of PMMI synthetized by free radical polymerization using dibenzoyl peroxide as initiator. It is observed that graphite is stable through the whole temperature range, where the total weight loss at 800 °C is only 1.8%. It is also observed that the thermogravimetric curve of graphite shows a slight weight increase, of less than 1%, during the heating process. This apparent weight gain is within the limits of uncertainty of TGA apparatus and can be related to buoyancy effects from the gas density decrease with increasing temperature [65]. Graphene oxide shows a drastic thermal decomposition at 270 °C, due to the degradation of oxygenated functional groups. This abrupt change indicates that this process occurs by deflagration, which different authors have explained as the process responsible of the exfoliation of graphite oxide in the production of thermally reduced graphene oxide [66]. Silanization of GO produces a material which is thermally less stable than GO, since the deflagration occurs near 200 °C [67]. This suggests the high potential energy of siloxane moieties successfully incorporated to GO. However, the GO-SB presents significant differences with GO and GO-S, since the decomposition process is observed around 300 °C. This could be associated to the degradation of organic functionalities as a result of the subsequent reactions with APTES and BIBB compounds. The weight loss during this process is around 10% and the lack of a degradation process around 200 °C indicates the occurrence of side reactions, such as the reduction of the oxygen groups, which competes with the nucleophilic substitution. This reduction promotes the loss of oxygenated functional groups, consequently the weight loss will be lower than that observed for GO-S. PMMI-g-GO shows two stages of degradation, the first stage around at 180 °C involves the dehydration of carboxylic acid moieties of PMMI, and the second stage at 300 °C is associated to the degradation of the PMMI covalently bonded to graphene layers. The similarity between the degradation curves of PMMI-g-GO and the control sample of PMMI indicates that the reaction of ARGET-ATRP was successfully achieved. The weight loss registered for PMMI-g-GO is 42.4%. This weight loss probably includes the loss of APTES-BIBB molecules from PMMI as well as those bonded to the GO surface. In this regard, by considering the weight loss registered for GO-SB, it is possible to estimate the molar ratio of MMI to APTES-BIBB as 7:1. This suggests that each APTES-BIBB section is covalently linked to a chain of seven repetitive monomeric units of MMI. However, in order to know the characteristic of this polymerization reaction, a further study for determining chain length and kinetics aspects should be attempted.

3.4. Electrical conductivity and macroscopic appearance of PMMI-g-GO

The electrical conductivity and dielectric permittivity of PMMI-g-GO as a function of frequency measured at room temperature are presented in Fig. 8. The AC electrical conductivity of the PMMI-g-GO presents the typical frequency-independent behavior of conductive materials, with a value of 5.04 S m^{-1} at 0.1 Hz. This high value of the electrical conductivity, compared to that of the GO sample of 10^{-6} Sm^{-1} at 0.1 Hz, is

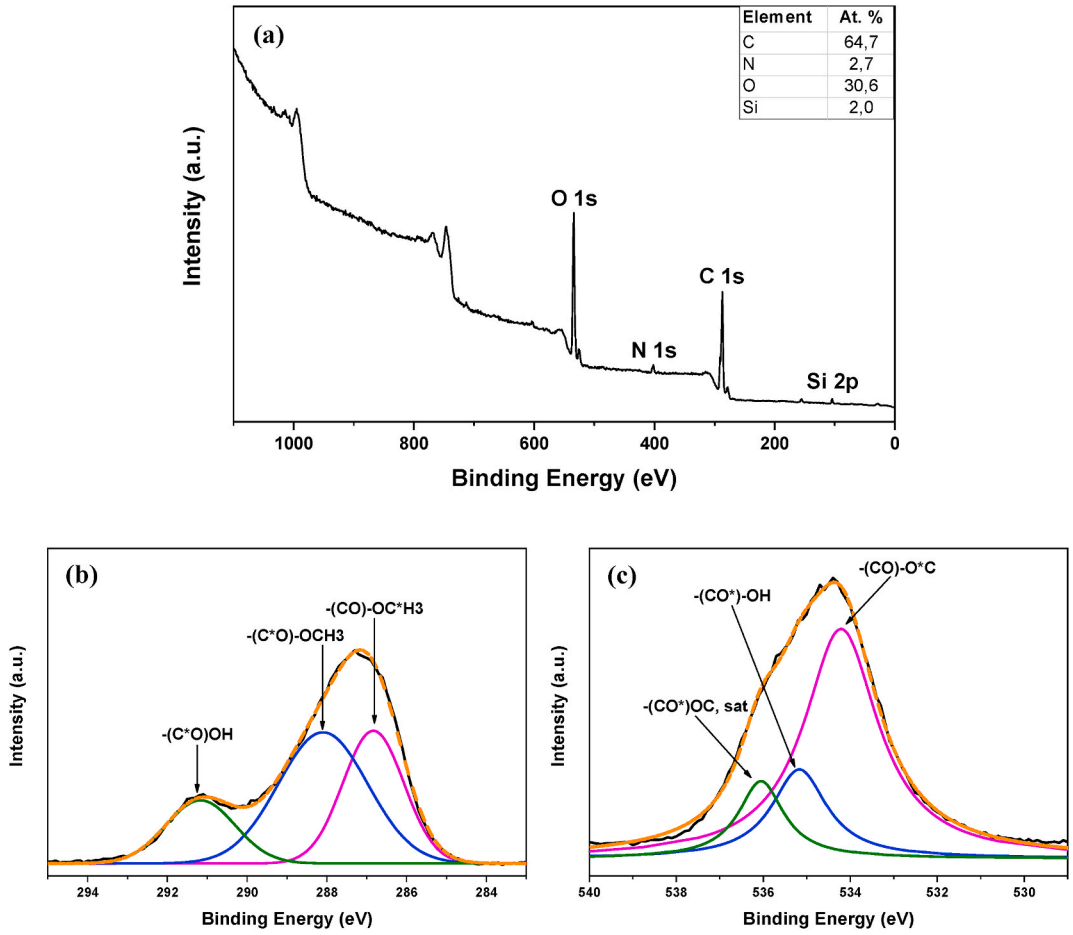

Fig. 5. XPS survey of PMMI-g-GO (a), deconvolution analysis of C1s (b) and O1s (c) of PMMI-g-GO. Symbol (*) indicates the specific atom in which the photoelectric effect is being observed.

attributed to the partial reduction of the GO sample mentioned above, and is consistent with the band structure of the graphenic materials [68]. The electronic conductivity is expected to be the most important contribution to electrical conductivity, as there is no evidence of an ionic contribution at low frequencies. In addition, it is observed that the dielectric permittivity decreases as the electric field frequency is increased, which has been associated to the interfacial polarization of graphene flakes [69,70].

In order to evaluate the performance of the PMMI-g-GO as potential electrode material for energy storage applications, a symmetric half-cell with lithium metal and PMMI-g-GO was assembled. Fig. 9 shows a sequence of galvanostatic charge/discharge cycles, showing a gravimetric capacity value for PMMI-g-GO up to 75 mA h/g when cycled at a current density of 1 mA/g. Although the coulombic efficiency (see the inset plot) seems to be dropping as the number of cycles increases, PMMI-g-GO shows a high lithium ion storage capacity. It is important to mention that the neat PMMI in combination with an electron conducting carbon additive, which was added due to the insulating nature of the polymer, was also galvanostatically cycled showing no redox activity or lithium ion storage capacity. This indicates that the storage capacity observed is due to GO grafted with PMMI since the non-modified GO has already been reported to have a poor performance as electrode material in lithium-ion batteries [71,72], due to the presence of functional oxygen-containing groups on the surface that results in a plethora of side reactions that cause the battery to fail. Thus, current graphene-based electrodes are based on reduced graphene oxide combined with another electroactive material or with carbon additives to improve their storage capacity properties [73–75]. Hence, this study presents for the first time that a multi-layer graphene oxide grafted with a polymer synthetized through a controlled radical polymerization using a monomer derived from renewable feedstock is reported. Nevertheless, the PMMI-g-GO capacity values are low compared with the theoretical values of graphite, which is 372 mA h/g, or that of reversible capacity (397.6 mA h/g) reported for graphite, using synthetic polymers, such as poly(vinyl difluoride) and poly(methyl methacrylate), as binder [76]. This fact indicates that the development of sustainable materials useful for energy storage applications, such as those based on itaconates feedstock, requires deeper study.

Finally, PMMI-g-GO presents interesting macroscopic features. For instance, it forms a colloidal gel particle when dispersed in water (Fig. 10a). The dry powder can be easily processed by applying pressure, resulting in a lightweight, ductile and electrically conductive film (Fig. 10b). This is not possible with conventional graphenic materials such as graphene oxide. These characteristics can facilitate the potential use of this material in a wide range of applications, as for instance, for ion capture in water, electrically conductive filler in polymers as well as electrode in batteries and supercapacitors.

4. Conclusions

Polymer brushes of high quality based on multi-layer graphene oxide grafted with poly (monomethyl itaconate) (PMMI-*g*-GO) have been successfully synthetized by atom transfer radical polymerization using activators regenerated by electron transfer (ARGET-ATRP). PMMI-g-GO has a low number of stacked layers (NL = 6) and recovers the π-conjugated system. It presents a high electrical conductivity of 5.04 S m^{-1} with

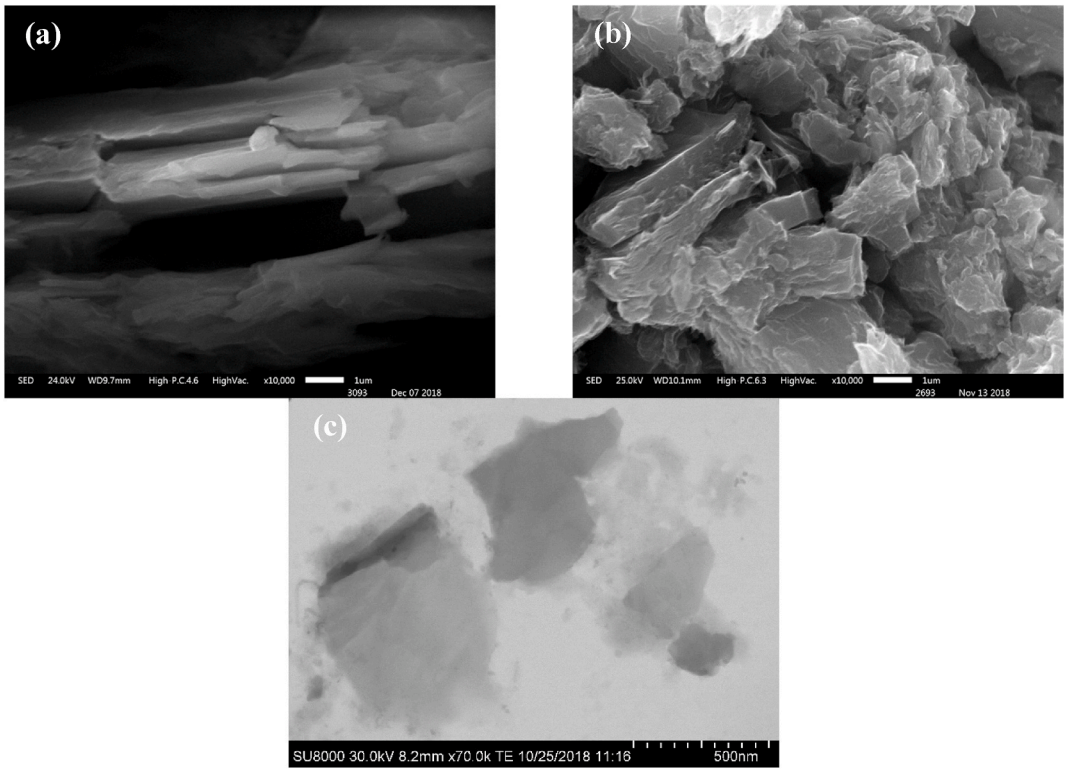

Fig. 6. SEM images of GO (a) and PMMI-g-GO (b) and STEM image of PMMI-g-GO (c).

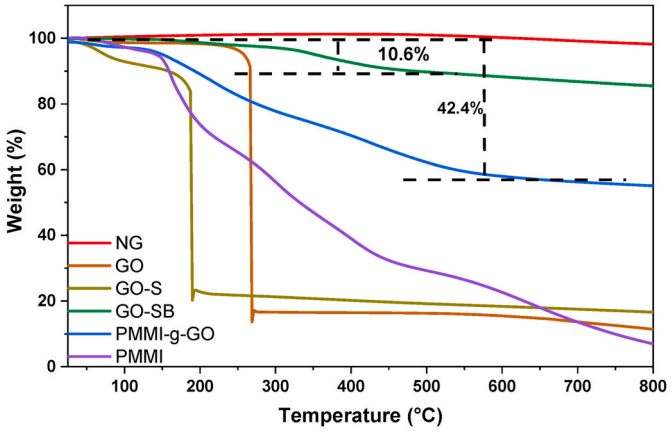

Fig. 7. Thermogravimetric analysis of the different graphenic materials and PMMI used as a control sample.

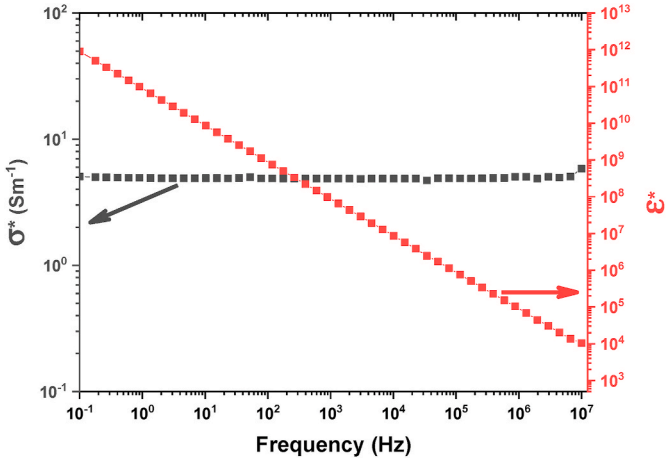

Fig. 8. Complex electrical conductivity (σ*) and complex dielectric permittivity (ε*) measured at room temperature as a function of frequency for PMMI-g-GO.

an Ohmic behavior. In addition, PMMI-g-GO exhibits interesting and versatile macroscopic characteristics, since it can form a colloidal gel when dispersed in water and as dry powder can be easily processed by applying pressure, resulting in a lightweight solid material. This material shows a high lithium ion storage capacity with gravimetric discharge capacity values of up to 75 mA h/g at a current density of 1 mA/g. This study demonstrates the potential application of this new nanomaterial using monomers from renewable resources as electrode material in energy storage and conversion applications and as conductive filler for multifunctional polymer composites.

CRediT authorship contribution statement

Héctor Aguilar-Bolados: Conceptualization, Methodology, Investigation, Writing - original draft, Writing - review & editing. **Mehrdad Yazdani-Pedram:** Conceptualization, Resources, Writing - review & editing. **Eduardo Quinteros-Jara:** Investigation. **Quimberly Cuenca-Bracamonte:** Investigation. **Raúl Quijada:** Resources. **Javier Carretero-González:** Methodology, Investigation, Writing - original draft, Writing - review & editing. **Francis Avilés:** Methodology, Investigation, Writing - review & editing. **Miguel A. Lopez-Manchado:** Conceptualization, Resources, Writing - review & editing. **Raquel Verdejo:** Conceptualization, Resources, Writing - original draft, Writing - review & editing.

Declaration of competing interest

The authors declare that they have no known competing financial

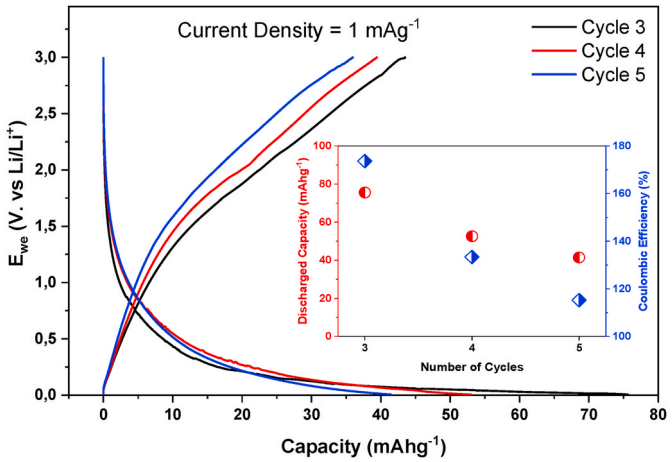

Fig. 9. Galvanostatic charge/discharge cycles of a lithium half-cell using PMMI-g-GO as electrode material.

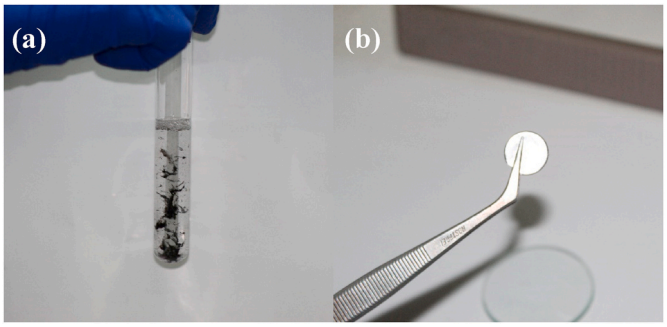

Fig. 10. PMMI-g-GO dispersed in water (a) and a disk obtained by pressing PMMI-g-GO at room temperature (b).

interests or personal relationships that could have appeared to influence the work reported in this paper.

Acknowledgements

This research was supported by the Chilean Agency for Research and Development (ANID) under Postdoctoral fellowship FONDECYT N° 3170104 granted to H. Aguilar-Bolados. H. Aguilar-Bolados also acknowledges to ANID the financial support under the grant FONDECYT project N°1200437. M Yazdani-Pedram, R. Quijada and H. Aguilar-Bolados acknowledge financial support from ANID through grant FONDECYT projects N° 1191566 and 1191642. R. Verdejo and M. A. Lopez-Manchado acknowledge the financial support from the MICI (grant number MAT2016-81138-R). Javier Carretero González acknowledges the Ramon y Cajal Fellow (RYC-2015-17722) from the MICI. The authors also thank Alejandro May-Pat for performing the AFM analysis. F. Avilés acknowledges the CONACYT infrastructure project N° 268595 for acquiring the AFM.

References

[1] H.W. Kroto, J.R. Heath, S.C. O'Brien, R.F. Curl, R.E. Smalley, C60: buckminsterfullerene, Nature 318 (1985) 162–163, https://doi.org/10.1038/318162a0.
[2] S. Iijima, Helical microtubules of graphitic carbon, Nature 354 (1991) 56–58, https://doi.org/10.1038/354056a0.
[3] K.S. Novoselov, A.K. Geim, S. V Morozov, D. Jiang, Y. Zhang, S. V Dubonos, I. V Grigorieva, A.A. Firsov, Electric field effect in atomically thin carbon films, Science 306 (2004) 666–669, https://doi.org/10.1126/science.1102896.
[4] S. Dimovski, Y. Gogotsi, 6 graphite whiskers, cones, and polyhedral crystals, Carbon Nanomater (2006), https://doi.org/10.1201/9781420009378.ch4 second ed.
[5] F. Perreault, A. Fonseca de Faria, M. Elimelech, Environmental applications of graphene-based nanomaterials, Chem. Soc. Rev. 44 (2015) 5861–5896, https://doi.org/10.1039/C5CS00021A.
[6] V.B. Mohan, K. Lau, D. Hui, D. Bhattacharyya, Graphene-based materials and their composites: a review on production, applications and product limitations, Compos. B Eng. 142 (2018) 200–220, https://doi.org/10.1016/j.compositesb.2018.01.013.
[7] S.K. Tiwari, S. Sahoo, N. Wang, A. Huczko, Graphene research and their outputs: status and prospect, J. Sci. Adv. Mater. Devices. 5 (2020) 10–29, https://doi.org/10.1016/j.jsamd.2020.01.006.
[8] A. Guirguis, J.W. Maina, X. Zhang, L.C. Henderson, L. Kong, H. Shon, L.F. Dumée, Applications of nano-porous graphene materials – critical review on performance and challenges, Mater. Horizons. 7 (2020) 1218–1245, https://doi.org/10.1039/C9MH01570A.
[9] A. Bianco, H.-M. Cheng, T. Enoki, Y. Gogotsi, R.H. Hurt, N. Koratkar, T. Kyotani, M. Monthioux, C.R. Park, J.M.D. Tascon, J. Zhang, All in the graphene family – a recommended nomenclature for two-dimensional carbon materials, Carbon N. Y. 65 (2013) 1–6, https://doi.org/10.1016/j.carbon.2013.08.038.
[10] V. Singh, D. Joung, L. Zhai, S. Das, S.I. Khondaker, S. Seal, Graphene based materials: past, present and future, Prog. Mater. Sci. 56 (2011) 1178–1271, https://doi.org/10.1016/j.pmatsci.2011.03.003.
[11] A.A. Balandin, Thermal properties of graphene and nanostructured carbon materials, Nat. Mater. 10 (2011) 569–581, https://doi.org/10.1038/nmat3064.
[12] S. Chen, Q. Wu, C. Mishra, J. Kang, H. Zhang, K. Cho, W. Cai, A.A. Balandin, R. S. Ruoff, Thermal conductivity of isotopically modified graphene, Nat. Mater. 11 (2012) 203–207, https://doi.org/10.1038/nmat3207.
[13] S. Chen, A.L. Moore, W. Cai, J.W. Suk, J. An, C. Mishra, C. Amos, C.W. Magnuson, J. Kang, L. Shi, R.S. Ruoff, Raman measurements of thermal transport in suspended monolayer graphene of variable sizes in vacuum and gaseous environments, ACS Nano 5 (2011) 321–328, https://doi.org/10.1021/nn102915x.
[14] E. Pop, V. Varshney, A.K. Roy, Thermal properties of graphene: fundamentals and applications, MRS Bull. 37 (2012) 1273–1281, https://doi.org/10.1557/mrs.2012.203.
[15] T. Chen, L. Pan, M. Lin, B. Wang, L. Liu, Y. Li, J. Qiu, K. Zhu, Dielectric, mechanical and electro-stimulus response properties studies of polyurethane dielectric elastomer modified by carbon nanotube-graphene nanosheet hybrid fillers, Polym. Test. 47 (2015) 4–11, https://doi.org/10.1016/j.polymertesting.2015.08.001.
[16] P.-G. Ren, X.-H. Liu, F. Ren, G.-J. Zhong, X. Ji, L. Xu, Biodegradable graphene oxide nanosheets/poly-(butylene adipate-co-terephthalate) nanocomposite film with enhanced gas and water vapor barrier properties, Polym. Test. 58 (2017) 173–180, https://doi.org/10.1016/j.polymertesting.2016.12.022.
[17] M. Wojtaś, D. V Karpinsky, M. V Silibin, S.A. Gavrilov, A. V Sysa, K.N. Nekludov, S. V Dubkov, Pyroelectricity in graphene oxide doped P(VDF-TrFE) films, Polym. Test. 71 (2018) 296–300, https://doi.org/10.1016/j.polymertesting.2018.09.013.
[18] G. Torğut, Fabrication, characterization of poly(MA-co-NIPA)-graphene composites and optimization the dielectric properties using the response surface method (RSM), Polym. Test. 76 (2019) 312–319, https://doi.org/10.1016/j.polymertesting.2019.03.035.
[19] M. Taj, S.R. Manohara, S.M. Hanagodimath, L. Gerward, Novel conducting poly (3,4-ethylenedioxythiophene) – graphene nanocomposites with gigantic dielectric properties and narrow optical energy band gap, Polym. Test. 90 (2020) 106650, https://doi.org/10.1016/j.polymertesting.2020.106650.
[20] P. Zhu, L. Weng, X. Zhang, X. Wang, L. Guan, J. Shi, L. Liu, Enhanced dielectric performance of TPU composites filled with Graphene@poly(dopamine)-Ag core-shell nanoplatelets as fillers, Polym. Test. 90 (2020) 106671, https://doi.org/10.1016/j.polymertesting.2020.106671.
[21] Y. Zhu, H. Ji, H.-M. Cheng, R.S. Ruoff, Mass production and industrial applications of graphene materials, Natl. Sci. Rev. 5 (2018) 90–101, https://doi.org/10.1093/nsr/nwx055.
[22] H. Aguilar-Bolados, D. Vargas-Astudillo, M. Yazdani-Pedram, G. Acosta-Villavicencio, P. Fuentealba, A. Contreras-Cid, R. Verdejo, M.A. López-Manchado, Facile and scalable one-step method for amination of graphene using leuckart reaction, Chem. Mater. 29 (2017), https://doi.org/10.1021/acs.chemmater.7b01438.
[23] H. Aguilar-Bolados, A. Contreras-Cid, M. Yazdani-Pedram, G. Acosta-Villavicencio, M. Flores, P. Fuentealba, A. Neira-Carrillo, R. Verdejo, M.A. López-Manchado, Synthesis of fluorinated graphene oxide by using an easy one-pot deoxyfluorination reaction, J. Colloid Interface Sci. 524 (2018) 219–226, https://doi.org/10.1016/j.jcis.2018.04.030.
[24] H. Aguilar-Bolados, J. Brasero, M.A. Lopez-Manchado, M. Yazdani-Pedram, High performance natural rubber/thermally reduced graphite oxide nanocomposites by latex technology, Compos. B Eng. 67 (2014), https://doi.org/10.1016/j.compositesb.2014.08.010.
[25] H. Kim, A.A. Abdala, C.W. Macosko, Graphene/polymer nanocomposites, Macromolecules 43 (2010) 6515–6530, https://doi.org/10.1021/ma100572e.
[26] P. Steurer, R. Wissert, R. Thomann, R. Mülhaupt, Functionalized graphenes and thermoplastic nanocomposites based upon expanded graphite oxide, Macromol. Rapid Commun. 30 (2009) 316–327, https://doi.org/10.1002/marc.200800754.
[27] R. Verdejo, F. Barroso-Bujans, M.A. Rodriguez-Perez, J. Antonio de Saja, M. A. Lopez-Manchado, Functionalized graphene sheet filled silicone foam nanocomposites, J. Mater. Chem. 18 (2008) 2221–2226, https://doi.org/10.1039/B718289A.
[28] H. Aguilar-Bolados, M. Yazdani-Pedram, R. Verdejo, Thermal, electrical, and sensing properties of rubber nanocomposites, High-Performance Elastomeric Mater, Reinf. by Nano-Carbons (2020) 149–175, https://doi.org/10.1016/B978-0-12-816198-2.00007-4.

[29] H.B. Kulkarni, P. Tambe, G.M. Joshi, Influence of covalent and non-covalent modification of graphene on the mechanical, thermal and electrical properties of epoxy/graphene nanocomposites: a review, Compos. Interfac. 25 (2018) 381–414, https://doi.org/10.1080/09276440.2017.1361711.
[30] J.O. Zoppe, N.C. Ataman, P. Mocny, J. Wang, J. Moraes, H.-A. Klok, Surface-initiated controlled radical polymerization: state-of-the-art, opportunities, and challenges in surface and interface engineering with polymer brushes, Chem. Rev. 117 (2017) 1105–1318, https://doi.org/10.1021/acs.chemrev.6b00314.
[31] A. Kumar, B. Behera, G.D. Thakre, S.S. Ray, Covalently grafted graphene oxide/poly(cn-acrylate) nanocomposites by surface-initiated ATRP: an efficient antifriction, antiwear, and pour-point-depressant lubricating additive in oil media, Ind. Eng. Chem. Res. 55 (2016) 8491–8500, https://doi.org/10.1021/acs.iecr.6b00848.
[32] N. Chan, M.F. Cunningham, R.A. Hutchinson, ARGET ATRP of methacrylates and acrylates with stoichiometric ratios of ligand to copper, Macromol. Chem. Phys. 209 (2008) 1797–1805, https://doi.org/10.1002/macp.200800328.
[33] G. Gonçalves, P.A.A.P. Marques, A. Barros-Timmons, I. Bdkin, M.K. Singh, N. Emami, J. Grácio, Graphene oxide modified with PMMA via ATRP as a reinforcement filler, J. Mater. Chem. 20 (2010) 9927–9934, https://doi.org/10.1039/C0JM01674H.
[34] M. Kumar, J.S. Chung, S.H. Hur, Controlled atom transfer radical polymerization of MMA onto the surface of high-density functionalized graphene oxide, Nanoscale Res. Lett. 9 (2014) 345, https://doi.org/10.1186/1556-276X-9-345.
[35] M. Mrlík, M. Ilčíková, T. Plachý, V. Pavlínek, Z. Špitalský, J. Mosnáček, Graphene oxide reduction during surface-initiated atom transfer radical polymerization of glycidyl methacrylate: controlling electro-responsive properties, Chem. Eng. J. 283 (2016) 717–720, https://doi.org/10.1016/j.cej.2015.08.013.
[36] Y. Lin, J. Jin, M. Song, Preparation and characterisation of covalent polymer functionalized graphene oxide, J. Mater. Chem. 21 (2011) 3455–3461, https://doi.org/10.1039/C0JM01859G.
[37] S.P. Lonkar, Y.S. Deshmukh, A.A. Abdala, Recent advances in chemical modifications of graphene, Nano Res 8 (2015) 1039–1074, https://doi.org/10.1007/s12274-014-0622-9.
[38] Y. Yang, J. Wang, J. Zhang, J. Liu, X. Yang, H. Zhao, Exfoliated graphite oxide decorated by PDMAEMA chains and polymer particles, Langmuir 25 (2009) 11808–11814, https://doi.org/10.1021/la901441p.
[39] M.A. Dubé, S. Salehpour, Applying the principles of green chemistry to polymer production technology, Macromol. React. Eng. 8 (2014) 7–28, https://doi.org/10.1002/mren.201300103.
[40] M.S. Lima, C.S.M.F. Costa, J.F.J. Coelho, A.C. Fonseca, A.C. Serra, A simple strategy toward the substitution of styrene by sobrerol-based monomers in unsaturated polyester resins, Green Chem. 20 (2018) 4880–4890, https://doi.org/10.1039/C8GC01214H.
[41] P. Li, S. Ma, J. Dai, X. Liu, Y. Jiang, S. Wang, J. Wei, J. Chen, J. Zhu, Itaconic acid as a green alternative to acrylic acid for producing a soybean oil-based thermoset: synthesis and properties, ACS Sustain. Chem. Eng. 5 (2017) 1228–1236, https://doi.org/10.1021/acssuschemeng.6b02654.
[42] B.C. Saha, G.J. Kennedy, M.J. Bowman, N. Qureshi, R.O. Dunn, Factors affecting production of itaconic acid from mixed sugars by Aspergillus terreus, Appl. Biochem. Biotechnol. 187 (2019) 449–460, https://doi.org/10.1007/s12010-018-2831-2.
[43] S. Saha, G.L. Baker, Substituent effects in surface-initiated ATRP of substituted styrenes, Appl. Surf. Sci. 359 (2015) 911–916, https://doi.org/10.1016/j.apsusc.2015.10.225.
[44] V.M.C. Coessens, K. Matyjaszewski, Fundamentals of atom transfer radical polymerization, J. Chem. Educ. 87 (2010) 916–919, https://doi.org/10.1021/ed1002256.
[45] H. Aguilar-Bolados, M. Yazdani-Pedram, M. Gallegos-Cofre, Highly electrical conductive composite material based on graphene-lithium polycarboxylate-nanoparticles, n.d. https://doi.org/PCT/IB2020/053864.
[46] L. Gargallo, D. Radic, M. Yazdani-Pedram, A. Horta, Properties of polyelectrolytes: poly(mono-methyl itaconate). conformational and viscometric behaviour in dilute solution, Eur. Polym. J. 25 (1989) 1059–1063, https://doi.org/10.1016/0014-3057(89)90137-7.
[47] A.C. Ferrari, D.M. Basko, Raman spectroscopy as a versatile tool for studying the properties of graphene, Nat. Nanotechnol. 8 (2013) 235–246, https://doi.org/10.1038/nnano.2013.46.
[48] S. Eigler, C. Dotzer, A. Hirsch, Visualization of defect densities in reduced graphene oxide, Carbon N. Y. 50 (2012) 3666–3673, https://doi.org/10.1016/j.carbon.2012.03.039.
[49] J.-B. Wu, M.-L. Lin, X. Cong, H.-N. Liu, P.-H. Tan, Raman spectroscopy of graphene-based materials and its applications in related devices, Chem. Soc. Rev. 47 (2018) 1822–1873, https://doi.org/10.1039/C6CS00915H.
[50] H.-J. Shin, S.M. Kim, S.-M. Yoon, A. Benayad, K.K. Kim, S.J. Kim, H.K. Park, J.-Y. Choi, Y.H. Lee, Tailoring electronic structures of carbon nanotubes by solvent with electron-donating and -withdrawing groups, J. Am. Chem. Soc. 130 (2008) 2062–2066, https://doi.org/10.1021/ja710036e.
[51] N. Bendiab, E. Anglaret, J.-L. Bantignies, A. Zahab, J.L. Sauvajol, P. Petit, C. Mathis, S. Lefrant, Stoichiometry dependence of the Raman spectrum of alkali-doped single-wall carbon nanotubes, Phys. Rev. B 64 (2001) 245424, https://doi.org/10.1103/PhysRevB.64.245424.
[52] B. Das, R. Voggu, C.S. Rout, C.N.R. Rao, Changes in the electronic structure and properties of graphene induced by molecular charge-transfer, Chem. Commun. (2008) 5155–5157, https://doi.org/10.1039/B808955H.
[53] W. Zhao, P.H. Tan, J. Liu, A.C. Ferrari, Intercalation of few-layer graphite flakes with FeCl3: Raman determination of fermi level, layer by layer decoupling, and stability, J. Am. Chem. Soc. 133 (2011) 5941–5946, https://doi.org/10.1021/ja110939a.
[54] M.G. Voronkov, A.Y. Deich, The donor-acceptor properties of the siloxane bond, J. Struct. Chem. 5 (1964) 443–448, https://doi.org/10.1007/BF00748884.
[55] A.C. Ferrari, Raman spectroscopy of graphene and graphite: disorder, electron–phonon coupling, doping and nonadiabatic effects, Solid State Commun. 143 (2007) 47–57, https://doi.org/10.1016/j.ssc.2007.03.052.
[56] Z.H. Ni, H.M. Wang, J. Kasim, H.M. Fan, T. Yu, Y.H. Wu, Y.P. Feng, Z.X. Shen, Graphene thickness determination using reflection and contrast spectroscopy, Nano Lett. 7 (2007) 2758–2763, https://doi.org/10.1021/nl071254m.
[57] P. Shivapooja, L.K. Ista, H.E. Canavan, G.P. Lopez, ARGET–ATRP synthesis and characterization of PNIPAAm brushes for quantitative cell detachment studies, Biointerphases 7 (2012) 1–9, https://doi.org/10.1007/s13758-012-0032-z.
[58] K. Endo, C. Inoue, N. Kobayashi, M. Aida, Spectra analysis of the XPS core and valence energy levels of polymers by an ab initio mo method using simple model molecules, J. Phys. Chem. Solid. 55 (1994) 471–478, https://doi.org/10.1016/0022-3697(94)90151-1.
[59] P. Laoharojanaphand, T.J. Lin, J.O. Stoffer, Glow discharge polymerization of reactive functional silanes on poly(methyl methacrylate), J. Appl. Polym. Sci. 40 (1990) 369–384, https://doi.org/10.1002/app.1990.070400306.
[60] F. Bournel, C. Laffon, P. Parent, G. Tourillon, Adsorption of some substituted ethylene molecules on Pt(111) at 95 K Part 1: NEXAFS, XPS and UPS studies, Surf. Sci. 350 (1996) 60–78, https://doi.org/10.1016/0039-6028(95)01254-0.
[61] R. Al-Gaashani, A. Najjar, Y. Zakaria, S. Mansour, M.A. Atieh, XPS and structural studies of high quality graphene oxide and reduced graphene oxide prepared by different chemical oxidation methods, Ceram. Int. 45 (2019) 14439–14448, https://doi.org/10.1016/j.ceramint.2019.04.165.
[62] G. Beamson, D.T. Clark, N.W. Hayes, D.S.-L. Law, Effect of crystallinity on the XPS spectrum of poly(ethylene terephthalate), Surf. Sci. Spectra 3 (1994) 357–365, https://doi.org/10.1116/1.1247788.
[63] B. Kartick, S.K. Srivastava, Simple facile route for the preparation of graphite oxide and graphene, J. Nanosci. Nanotechnol. 11 (n.d.) 8586–8592. https://www.ingentaconnect.com/content/asp/jnn/2011/00000011/00000010/art00023.
[64] S.H. Lee, D.R. Dreyer, J. An, A. Velamakanni, R.D. Piner, S. Park, Y. Zhu, S.O. Kim, C.W. Bielawski, R.S. Ruoff, Polymer brushes via controlled, surface-initiated atom transfer radical polymerization (ATRP) from graphene oxide, Macromol. Rapid Commun. 31 (2010) 281–288, https://doi.org/10.1002/marc.200900641.
[65] N. Saadatkhah, A. Carillo Garcia, S. Ackermann, P. Leclerc, M. Latifi, S. Samih, G. S. Patience, J. Chaouki, Experimental methods in chemical engineering: thermogravimetric analysis—TGA, Can. J. Chem. Eng. 98 (2020) 34–43, https://doi.org/10.1002/cjce.23673.
[66] Y. Qiu, F. Guo, R. Hurt, I. Külaots, Explosive thermal reduction of graphene oxide-based materials: mechanism and safety implications, Carbon N. Y. 72 (2014) 215–223, https://doi.org/10.1016/j.carbon.2014.02.005.
[67] T. Serodre, N. Oliveira, D. Miquita, M. Ferreira, A. Santos, V. Resende, C. Furtado, T. Serodre, N.A.P. Oliveira, D.R. Miquita, M.P. Ferreira, A.P. Santos, V.G. Resende, C.A. Furtado, Surface silanization of graphene oxide under mild reaction conditions, J. Braz. Chem. Soc. 30 (2019) 2488–2499, https://doi.org/10.21577/0103-5053.20190167.
[68] B. Partoens, F.M. Peeters, From graphene to graphite: electronic structure around the *K* point, Phys. Rev. B 74 (2006) 75404, https://doi.org/10.1103/PhysRevB.74.075404.
[69] L.J. Romasanta, M. Hernández, M.A. López-Manchado, R. Verdejo, Functionalised graphene sheets as effective high dielectric constant fillers, Nanoscale Res. Lett. 6 (2011) 508, https://doi.org/10.1186/1556-276X-6-508.
[70] M. Martin-Gallego, M. Hernández, V. Lorenzo, R. Verdejo, M.A. Lopez-Manchado, M. Sangermano, Cationic photocured epoxy nanocomposites filled with different carbon fillers, Polymer 53 (2012) 1831–1838, https://doi.org/10.1016/j.polymer.2012.02.054.
[71] V.S. Channu, R. Bobba, R. Holze, Graphite and graphene oxide electrodes for lithium ion batteries, Colloids Surfaces A Physicochem. Eng. Asp. 436 (2013) 245–251, https://doi.org/10.1016/j.colsurfa.2013.06.018.
[72] C. Zhao, H. Gao, C. Chen, H. Wu, Reduction of graphene oxide in Li-ion batteries, J. Mater. Chem. A. 3 (2015) 18360–18364, https://doi.org/10.1039/C5TA05068E.
[73] J. Shim, D.-G. Kim, H.J. Kim, J.H. Lee, J.-H. Baik, J.-C. Lee, Novel composite polymer electrolytes containing poly(ethylene glycol)-grafted graphene oxide for all-solid-state lithium-ion battery applications, J. Mater. Chem. A. 2 (2014) 13873–13883, https://doi.org/10.1039/C4TA02667E.
[74] M. Li, H. Song, X. Chen, J. Zhou, Z. Ma, Phenolic resin-grafted reduced graphene oxide as a highly stable anode material for lithium ion batteries, Phys. Chem. Chem. Phys. 17 (2015) 3250–3260, https://doi.org/10.1039/C4CP04556D.
[75] Y. Li, Z. Jian, M. Lang, C. Zhang, X. Huang, Covalently functionalized graphene by radical polymers for graphene-based high-performance cathode materials, ACS Appl. Mater. Interfaces 8 (2016) 17352–17359, https://doi.org/10.1021/acsami.6b05271.
[76] Y. Wang, H. Zheng, Q. Qu, L. Zhang, V.S. Battaglia, H. Zheng, Enhancing electrochemical properties of graphite anode by using poly(methylmethacrylate)–poly(vinylidene fluoride) composite binder, Carbon N. Y. 92 (2015) 318–326, https://doi.org/10.1016/j.carbon.2015.04.084.